On the recent elevation changes at the Flade Isblink Ice Cap, northern Greenland

E. J. Rinne,[1] A. Shepherd,[2] S. Palmer,[2] M. R. van den Broeke,[3] A. Muir,[4] J. Ettema,[5] and D. Wingham[4]

Received 21 January 2011; revised 21 May 2011; accepted 6 July 2011; published 21 September 2011.

[1] We have used Radar Altimeter 2 (RA-2) onboard ESA's EnviSAT and Geosciences Laser Altimeter System (GLAS) onboard NASA's ICESat to map the elevation change of the Flade Isblink Ice Cap (FIIC) in northern Greenland. Based on RA-2 data we show that the mean surface elevation change of the FIIC has been near zero (0.03 ± 0.03 m/a) between fall 2002 and fall 2009. We present the elevation change rate maps and assess the elevation change rates of areas above the late summer snow line (0.09 ± 0.04 m/a) and below it (−0.16 ± 0.05 m/a). The GLAS elevation change rate maps show that some outlet glaciers, previously reported to have been in a surge state, are thickening rapidly. Using the RA-2 measured average elevation change rates for different parts of the ice cap we present a mass change rate estimate of 0.0 ± 0.5 Gt/a for the FIIC. We compare the annual elevation changes with surface mass balance (SMB) estimates from a regional atmospheric climate model RACMO2. We find a strong correlation between the two (R = 0.94 and P < 0.002), suggesting that the surface elevation changes of the FIIC are mainly driven by net SMB. The correlation of modeled net SMB and measured elevation change is strong in the southern areas of the FIIC (R = 0.97 and P < 0.0005), but insignificant in the northern areas (R = 0.38 and P = 0.40). This is likely due to higher variability of glacier flow in the north relative to the south.

Citation: Rinne, E. J., A. Shepherd, S. Palmer, M. R. van den Broeke, A. Muir, J. Ettema, and D. Wingham (2011), On the recent elevation changes at the Flade Isblink Ice Cap, northern Greenland, *J. Geophys. Res.*, *116*, F03024, doi:10.1029/2011JF001972.

1. Introduction

[2] Ice caps and glaciers are important present-day indicators of the ongoing global climate change. These bodies of ice are currently experiencing rapid changes. *Meier et al.* [2007] estimated the contribution from glaciers and ice caps to the global sea level rise in 2006 to have been 1.1 ± 0.24 mm/a when the total observed sea level rise was 3.1 ± 0.7 mm/a. In addition to the ice caps and glaciers the major contributors to the sea level rise are ice wastage from the ice sheets (0.5 mm/a) and the steric effect of ocean warming (1.6 mm/a) [*Meier et al.*, 2007]. Future projections predict significant volume loss rate from ice caps and glaciers for the next century: according to a multimodel study by *Radić and Hock* [2010], the sea level rise from glaciers and ice caps will amount to 12.4 ± 3.7 cm by 2100. This equates to loss of one fifth of the whole volume of ice in glaciers and ice caps today.

[3] The total sea level rise potential of glaciers and ice caps is altogether an order of magnitude smaller than that of the massive continental ice sheets. The ice loss rate from the Greenland ice sheet (GrIS) is increasing and combined with that of the Antarctic ice sheet may already have exceeded the mass loss rate from glaciers and ice caps [*Rignot et al.*, 2011]. However, the contribution of ice caps and glaciers will stay significant during the next century. Also, because systems of different size will react differently to rising global temperatures, the study of all land ice bodies is vital in the context of global warming.

[4] The surface mass balance (SMB) of an ice cap is determined by climate, mostly by precipitation and surface energy balance. These govern the rates of accumulation and ablation, respectively. A change in climate affects the rates of snow accumulation and ablation of the ice caps which, in turn, may lead to changes in their surface elevation. Other processes, such as iceberg calving and changes in ice and snow density, will also have an effect on the ice cap surface elevation.

[5] Recent satellite altimeters, such as the Radar Altimeter 2 (RA-2) [*Resti et al.*, 1999] and the Geosciences Laser

[1]School of GeoSciences, University of Edinburgh, Edinburgh, UK.
[2]School of Earth and Environment, University of Leeds, Leeds, UK.
[3]Institute for Marine and Atmospheric Research, Utrecht University, Utrecht, Netherlands.
[4]Centre for Polar Observation and Modeling, University College of London, London, UK.
[5]Faculty of Geo-Information Science and Earth Observation (ITC), University of Twente, Enschede, Netherlands.

0148-0227/11/2011JF001972

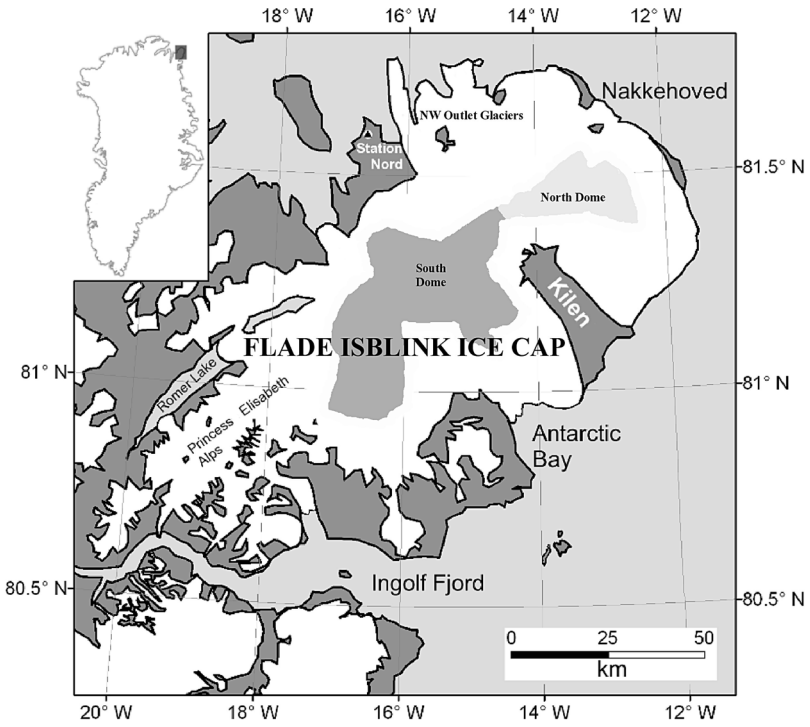

Figure 1. Location and map of the FIIC. South and North domes combined are the flat area of surface slopes <3%.

Altimeter System (GLAS) [*Zwally et al.*, 2002], provide near-global data sets of surface elevation. These data can be applied to surface elevation change studies of land ice masses. Satellite measurements provide extensive spatial and temporal coverage of the remote and rarely visited areas, that in practice cannot be monitored by other means.

[6] Flade Isblink Ice Cap (FIIC) is located in North-East Greenland (Figure 1). It covers an area of 8500 km^2, which makes it the largest ice cap in Greenland separate from the GrIS [*Kelly and Lowell*, 2009]. The FIIC is characterized by low surface slopes in its north-east part, and steeper slopes as well as some nunataks in the south-west part, which overlays the Princess Elisabeth Alps. The maximum elevation of the FIIC is approximately 960 m and the ice thickness close to the central summit is 535 m. The weather patterns of the FIIC are controlled by moisture and heat from the ice-free ocean to the east, and cold dry winds from the north-west [*Rasmussen*, 2004]. The FIIC forces the cold north-westerly air mass upwards into the warmer moist air mass originating from the ice-free eastern side. When these air masses meet, precipitation falls on the western side of the FIIC, while the eastern side is sheltered and receives less snow [*Rasmussen*, 2004].

[7] The outlet glaciers of the FIIC have experienced several advances and retreats. Radiocarbon dating of glacially overrun sediments show that the FIIC glaciers advanced sometime after 7800 BP, but have retreated since [*Hjort*, 1997]. Some model studies suggest the present-day FIIC to be a young ice mass – only some thousands of years old, much like the Hans Tausen Ice Cap to the west of the FIIC (A. Lemark, personal communication, 2009). Plant remains dated to 1510–1600 AD were also found to have been overrun by the margin of the FIIC, suggesting that the FIIC has advanced as recently as during the Little Ice Age [*Hjort*, 1997].

[8] There have been two previous studies describing surface elevation changes at the FIIC [*Krabill et al.*, 2000; *Pritchard et al.*, 2009]. Both of these studies concentrated on the GrIS, but they also included elevation change estimates for the FIIC. *Krabill et al.* [2000] conducted aircraft laser altimeter campaigns in Greenland for the years 1994 and 1999. Their repeat measurements along two intersecting flight lines over the FIIC show a thickening of 0.4–0.6 m/a across most of the ice cap surface, with a small area of thinning near the eastern margin. The fastest thickening was observed in the south-western part of the FIIC [*Krabill et al.*, 2000]. *Pritchard et al.* [2009] used the GLAS to examine elevation changes of the GrIS, but also included the FIIC in their study domain. They found that between 2003 and 2007, the western half of the FIIC thickened by around 0.5 m/a and the eastern half thinned by around 0.2 m/a. Because the main target of both studies was the GrIS, the chosen spatial resolution of their elevation change maps did not resolve the details of the FIIC elevation changes [*Pritchard et al.*, 2009; *Krabill et al.*, 2000].

[9] In this paper we assess the elevation change of the FIIC for the years 2002 to 2009 using two satellite altimeters: RA-2 and GLAS. Maps of the elevation change rates of the FIIC are presented for the time period 2004–2008. We also compare annual RA-2 elevation change measurements with the modeled net SMB estimates from the regional climate model RACMO2. This way we can

assess the recent mass changes of FIIC, as well as the role and importance of SMB in the evolution of FIIC surface elevation.

2. Methodology

[10] To assess the elevation change of FIIC we used two independent satellite altimeters: GLAS that flew with NASA's Ice, Cloud and land Elevation satellite (ICESat) [*Zwally et al.*, 2002], and RA-2 flying onboard ESA's Environmental satellite (EnviSAT) [*Resti et al.*, 1999]. The two altimeters operate at different frequencies, GLAS being a laser altimeter and RA-2 a radar altimeter. They complement each other in both temporal and spatial resolution. The RA-2 hasa large beam-limited footprint of 19 km [*Resti et al.*, 1999]. Although the pulse-limited ground footprint of RA-2 is considerably smaller than this [*Soussi and Femenias*, 2006], the spatial resolution of RA-2 is still two orders of magnitude poorer than that of GLAS, which has a footprint is only about 70 m [*Zwally et al.*, 2002]. The advantage of RA-2 is that it provides measurements independent of cloud conditions, whereas clouds limited the GLAS data acquisition. Furthermore, GLAS only obtained measurements during two or three periods per year. At a given point under an ICESat ground track on the FIIC, there were on average 4.1 successful GLAS measurements during 2004–2008. For the same period, the RA-2 provided an average of 31.9 successful measurements per crossover point on the FIIC.

2.1. ICESat GLAS

[11] GLAS provided near global (86°N to 86°S latitude) surface elevation measurements from February 2003 until the failure of the last laser in October 2009. One of the major challenges in obtaining elevation change estimates from GLAS data is the local cross-track slope estimate requirement. The ground tracks of ICESat from different years may have a spacing of up to 100 m at the FIIC. As a result, even a reasonably small cross-track slope of 2% creates a 2 m difference in elevations measured during different tracks. This is larger than the expected elevation change signal, and therefore the effect of the cross-track slope has to be removed from the measured elevation values.

[12] A method to estimate the cross-track slope, known as plane fitting, was used by *Pritchard et al.* [2009]. They calculated the average cross-track slope for all measured track pairs during 2003, and used this to compensate for surface slope in later measurements. For our slope correction we use a high precision (better than 10 cm) digital elevation model (DEM), formed using interferometric synthetic aperture radar (InSAR) data acquired by the European Remote Sensing (ERS) satellite in winter 1996 [*Palmer et al.*, 2010]. As InSAR-derived height maps contain relative values only, absolute surface elevation can only be retrieved with the use of tie-points of known elevation [*Nielsen et al.*, 1997]. For the FIIC DEM this retrieval is achieved by applying a least squares fit of the unwrapped phase at 500 points of known elevation, measured by GLAS in 2007 [*Palmer et al.*, 2010]. Thus, the FIIC DEM we utilize is not independent of the GLAS data used in this study. However, in our analysis of GLAS data we only use the slope information from the DEM and not the absolute height. Therefore the dependence of FIIC DEM on GLAS data does not impede the quality of our elevation change estimates.

[13] The GLAS data used in this paper is the GLAS/ICESat L1B Global Elevation Data set or GLA06, available free of charge online from the National Snow and Ice Data Center (NSIDC) [*Zwally et al.*, 2003]. Saturation correction was added to the elevations. Data points with no saturation elevation correction or large receiver gain values (greater than 150) were discarded. Geolocations in the GLA06 data set were used without additional corrections.

[14] To assess the elevation change of the ice surface, we calculated the difference (Δh (x, t)) between GLAS measured elevations $h(x,t)$ and our DEM (h_{DEM}). Both the GLAS measured and DEM elevations were in reference to the ICESat/GLAS geoid. We calculated the average $\Delta h(x, t)$ for x inside 1 km^2 data bins for each operations period:

$$\Delta h(x,t) = \frac{\sum_{i=1}^{n} h_i(x,t) - h_{DEM}(x)}{n} \quad (1)$$

[15] If the local features present in the GLAS data are resolved by the DEM, the Δh is the sum of three factors: error in DEM (for example due to radar penetration), GLAS instrument error, and actual physical changes in surface elevation between the time of the InSAR study and the GLAS measurement. To obtain an elevation trend, we fitted a first degree polynomial to these elevation differences, so that the slope of the polynomial represents the elevation trend in the data bin. For the elevation trend map, the elevation trends were then interpolated by a bicubic spline method [*Sandwell*, 1987] to obtain elevation trends between ICESat tracks where no measurements were available. Average elevation trends for large areas were calculated from non-interpolated measurements.

[16] We did not calculate a formal error estimate for each elevation measurement, because too many of the contributory factors (surface roughness, change of the surface topography since the DEM was measured, etc.) are poorly known. Instead we use the 1-σ confidence interval provided by the regression of the trend. Similar error estimate based on variation of the elevation measurements has been used in the past for example by *Wingham et al.* [1998]. There is a known GLAS inter-campaign bias that adds a systematic error to measured elevation change rates. Magnitude of the trend of this bias has been estimated to be of the order of 0.006 m/a by *Zwally et al.* [2011]. Due to this error contribution, we added 0.01 m/a to our GLAS uncertainty estimates.

2.2. EnviSAT RA-2

[17] To assess the elevation change rate from RA-2, we employed the dual crossover method previously used to assess the elevation change of the Antarctic Ice Sheet [*Wingham et al.*, 1998], GrIS [*Thomas et al.*, 2008] and the Devon Ice Cap [*Rinne et al.*, 2011]. The method is based on the *dh*/*dt* -method introduced by *Zwally et al.* [1989]. In the dual crossover method only crossovers with two pairs of tracks (see equation (2)) are used.

[18] The foundation of our RA-2 processing is to define the change in elevation, $\Delta h\ (x, t, t_{ref})$, in orbital crossover points x between times t and t_{ref}:

$$\Delta h(x,t,t_{ref}) = \left[\frac{(h_{At} - h_{Dtref}) + (h_{Atref} - h_{Dt})}{2}\right]_{t=t1\ldots tN} \quad (2)$$

[19] h_{At} and h_{Dt} refer to elevations measured during ascending and descending passes, respectively. Using the average of two different geometry crossovers removes the possible ascending versus descending biases in radar penetration [*Arthern et al.*, 2001]. In this manner, we get a time series of $\Delta h\ (x, t, t_{ref})$. To reduce noise, values of $\Delta h\ (x, t, t_{ref})$ are binned into 10 *km* by 10 *km* cells (data bins) and then averaged.

[20] The choice of the reference time t_{ref} affects the resulting time series $\Delta h\ (x, t, t_{ref})$. As we are calculating the change in elevation, and not the absolute elevation, we can choose an arbitrary point in time (within our measurement period) as our reference. In practice a choice of one reference point in time is not enough, as a measurement from a certain point in time may lack some coverage over the study area. Also there are errors inherent in every measurement, and choosing just one reference point may introduce bias into the resulting time series.

[21] Instead, we used ten different time periods (ten orbital cycles of 35 days) as references. We assume the elevation change during one orbital cycle to be negligible. Every chosen reference cycle yields a slightly different time series of $\Delta h\ (x, t, t_{ref})$. The time series using different reference cycles were finally combined into one, which reduces the uncertainty and leads to a better coverage of the study area.

[22] The individual time series, in reference to different orbital cycles, have a different placement regards to the level of zero elevation change. Before their combination, a constant value was added to each time series. Adding this constant (which assumed a different value for each time series) adjusted each time series so that it was in reference to the same level of zero elevation change. The value of this constant was optimized so that the square sum of differences between the time series (after adding the constant) and the time series with most data points was minimized.

[23] Finally, a first degree polynomial $P_{\Delta h}$ was fitted to the combined time series of $\Delta h\ (x, t)$ in each bin. The slope of $P_{\Delta h}$ represents the elevation change rate *dh/dt*. The overall trend is determined from the slope of a first degree polynomial, even if the elevation change of the ice surface is not always linear. Although we could have used the difference of the first and last elevation measurement (being analogous to two altimeter campaigns at different times), our chosen method is less sensitive to error in single measurements or anomalous circumstances during one of the measurements times.

[24] The largest error sources contributing to the radar altimeter measurement are radar speckle (associated with sub-footprint surface topography) and time-variant penetration of the radar signal into the snowpack [*Arthern et al.*, 2001].To minimize the variation of radar penetration, we only use RA-2 measurements from times when the snow surface is wet and the radar penetration is negligible. *Hall et al.* [2008] compared satellite-based Moderate Resolution Imaging Spectroradiometer (MODIS) measurements of surface temperature to in situ observations and found that there was no variation in surface temperature with elevation on 3 July 2001 and on 23 June 2004, suggesting that the entire ice surface of the FIIC was at or near to melting on these dates. We only use RA-2 measurements made between late summer and early fall (start of July and mid-September).

[25] Because we compared RA-2 measurements with other RA-2 measurements only, we did not apply a slant-range correction. Furthermore, we chose not to apply the re-location of measurement. Due to this, the actual location of radar echo is upslope from the nadir point. In consequence, we can't measure the very lowest elevations of the ice cap. All of the error sources are functions of time and location and, in general, are poorly known – especially on an ice surface with non-zero slopes. Analogously to GLAS, in the absence of formal estimates of error for the RA-2 over ice caps, we use the 1-σ confidence interval provided by the regression of the trend as our change rate uncertainty estimate.

2.3. RACMO2 Climate Model

[26] The Regional Atmospheric Climate Model (RACMO2/GR) was applied over a domain that includes the GrIS and its surrounding oceans and islands at high horizontal resolution of 11 km. For use over Greenland, RACMO2 has been coupled to a physical snow model that explicitly treats properties of snow, firn and ice, meltwater percolation, retention and refreezing [*Bougamont et al.*, 2005; *Ettema et al.*, 2009]. The atmospheric part of the model is forced at the lateral boundaries and the sea surface by the interim-reanalysis of the ECMWF (European Centre for Medium-Range Weather Forecasts, ERA-Interim, 1989–2009). *Ettema et al.* [2009, 2010] showed that RACMO2/GR accurately simulates the present-day climate of the GrIS: present-day SMB correlates well with observations from snow pits and snow cores (r = 0.95), resulting in credible estimates of recent Greenland mass losses [*van den Broeke et al.*, 2009]. We used the (1-σ) uncertainty estimate e_{RACMO2} by *Ettema et al.* [2009] for RACMO2 modeled net SMB values of:

$$e_{RACMO2} = 15 + 0.01 * SMB + 0.0002 * SMB^2 \left[\mathrm{kg/m^2}\right] \quad (3)$$

3. Results and Discussion

[27] The elevation change rates between 2004 and 2008 are presented in Figures 2 (GLAS) and 3 (RA-2). We have plotted the RA-2 measured elevation change rates for 2004–2008, instead of the whole RA-2 data period, to allow cross-comparison of the two altimeters.

[28] The elevation change rate maps from these two independent instruments show similar features: elevation gain over most of the FIIC, with elevation loss in the low elevation areas and in the northern dome area. The RA-2 measured an average elevation change rate of 0.03 ± 0.03 m/a from fall 2002 to fall 2009. For the period 2004 to 2008, RA-2 measured an average elevation change rate of 0.10 ± 0.07 m/a and the GLAS measured an average elevation change rate of

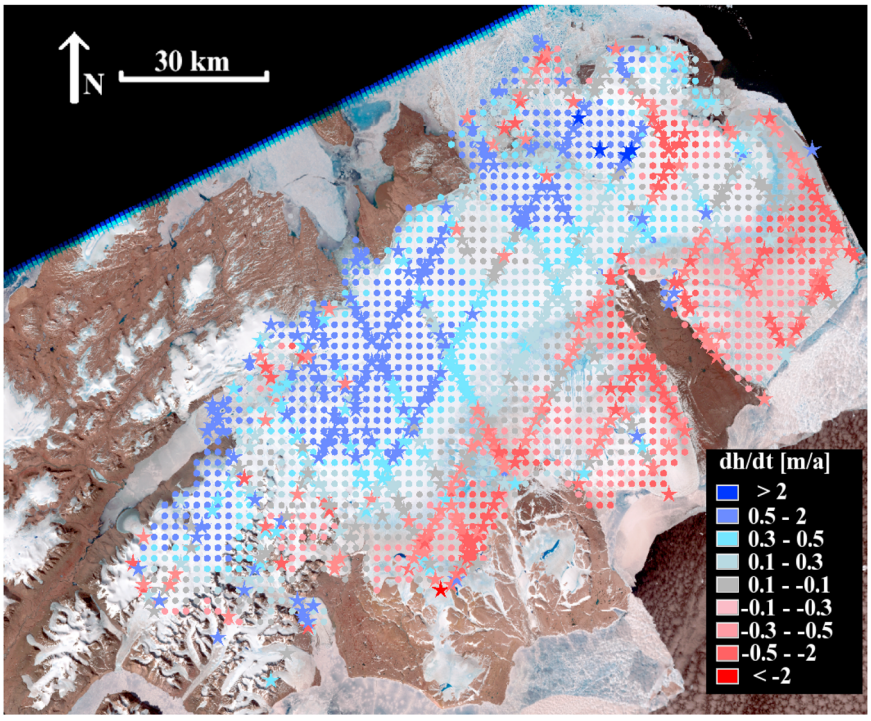

Figure 2. Elevation change rate map from GLAS (2004–2008). Stars are GLAS measured values, small circles interpolated values. Background: Landsat ETM+ scene from July 2001 (NASA).

0.17 ± 0.23 m/a. The RA-2 derived elevation change rate is within the uncertainty of the GLAS elevation change rate.

[29] The fine spatial resolution of the GLAS allowed us to study the spatial variation of the elevation change rates of the FIIC during 2004–2008 (see Figure 2). The observations show a clear pattern of elevation change over the ice cap: the western area has been gaining elevation at rates of up to more than 2 m/a, whereas areas in the east have been losing

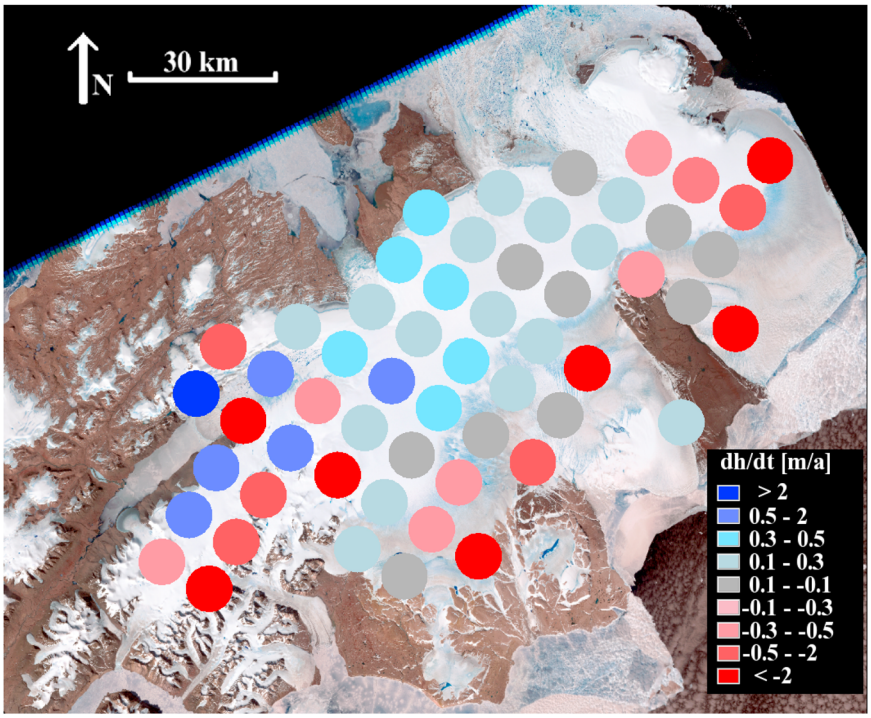

Figure 3. Elevation change rate map from RA-2 (2004–2008). The circles are the 10 km by 10 km RA-2 data bins. Background: Landsat ETM+ scene from July 2001 (NASA).

Table 1. Elevation and Mass Change Rates of the FIIC

	Above LSSL dh/dt [m/a]	Below LSSL dh/dt [m/a]	Whole FIIC dh/dt [m/a]	Above LSSL dM/dt [Gt/a]	Below LSSL dM/dt [Gt/a]	Whole FIIC dM/dt [Gt/a]
GLAS (2004–2008)	0.27 ± 0.29	−0.24 ± 0.23	0.17 ± 0.28	1.4 ± 1.5	−0.7 ± 0.7	0.7 ± 1.8
RA-2 (2004–2008)	0.16 ± 0.10	−0.11 ± 0.05	0.10 ± 0.07	0.3 ± 0.2	−0.8 ± 0.6	−0.5 ± 0.8
RA-2 (2002–2009)	0.09 ± 0.04	−0.16 ± 0.05	0.03 ± 0.03	0.4 ± 0.3	−0.4 ± 0.2	0.0 ± 0.5

elevation at rates up to 1 m/a. The negative elevation change rates are concentrated on the low elevation ablation areas of the ice cap. Our RA-2 measurements presented in Figure 3 confirm this elevation change pattern of the FIIC.

[30] To quantify elevation changes above and below Late Summer Snow line (LSSL), we applied a semi-automated LSSL retrieval algorithm to a Landsat ETM+ frame from July 2001 (a year with typical SMB according to RACMO2). We used the LSSL to calculate the average elevation rates for the area of the FIIC that was snow covered in July 2001, as well as for areas of bare ice. Average elevation change rates and corresponding mass changes are presented in Table 1. The FIIC was not only increasing in mean elevation during 2004–2008, but its geometry was also changing: accumulation areas of the FIIC increased in elevation and ablation areas decreased in elevation. Our elevation change rate map (Figure 2) agrees with the map of elevation change rates by *Pritchard et al.* [2009] (using the same data set but a different algorithm), but has a better spatial resolution. Elevation change rates mapped by GLAS are also similar to those mapped by a repeat airborne altimetry study in 1994 and 1999 [*Krabill et al.*, 2000].

[31] Closer inspection of the GLAS-measured elevation change reveals that three outlet glaciers north-east of Station Nord gained elevation faster than the surrounding areas. Based on a study of satellite measured velocities from 2000–2001 and 2005–2006, *Joughin et al.* [2010] reported a large (from 300 m/a to 60 m/a) slowdown of the largest two of these glaciers. Several large longitudinal crevasses and digitate termini, both characteristics of a surging glacier [*Copland et al.*, 2003], are visible in the Landsat ETM+ image acquired in July 2001. This implies that the glaciers were in surge state during 2000, and that the surge had ended by 2005. Thickening of these glaciers could be explained by slowdown in the glacier flow.

[32] The drainage area of the northernmost glacier (northern dome) is also a notable exception to the general pattern of increasing elevation at areas above the LSSL. Both GLAS and RA-2 measure an elevation loss in this area. The airborne study by *Krabill et al.* [2000] found this area to have been thickening during 1994–1999, in a similar manner to other high elevation areas of the FIIC. We suggest that the 2004–2008 decrease in the northern dome surface elevation results from increased ice flow from the upper areas to the lower areas of the glacier after a surge of the outlet glacier.

[33] Based on the GLAS observations the thickening of some parts of the FIIC is among the fastest in Greenland. The largest observed thickening rate on FIIC was 3.4 ± 0.7 m/a. In addition to the peak thickening rate, a 1800 km^2 area thickened faster than 0.5 m/a. Thickening rates of this magnitude are not common on GRiS. *Pritchard et al.* [2009] found dynamic thickening rates similar to those we have observed on FIIC only on two quiescent phase outlet glaciers, Storsstrommen and L. Bistrup Brae, both in North-East Greenland. In contrast, thinning rates we observe below the LSSL of FIIC are common in the margins of GrIS [*Pritchard et al.*, 2009].

[34] To estimate the net mass change rate of the FIIC, we first calculated the average elevation change rate for the area above the LSSL (5848 km^2) and for the area below it (3001 km^2) (see Table 1). These rates were 0.09±0.04 m/a and −0.16 ± 0.05 m/a, respectively. We assume the elevation gain above the LSSL to be due to thickening firn (average density of 660 ± 250 kg/m^3), and elevation loss below the LSSL to be due to loss of ice (average density of 900 ± 10 km/m^3). The same density values were used by *Gardner et al.* [2011] to derive mass change estimates from GLAS measured elevation changes of ice caps in Canadian Arctic archipelago. Firn compaction models for large ice sheets have been previously used [e.g., *Zwally et al.*, 2005] to better estimate fluctuations in firn density, but these have not been validated on ice caps like the FIIC. Thus we have to accept the large uncertainty of our firn density above the LSSL, which also accounts for possible firn compaction. We did not account for glacial isostatic adjustment, since the resulting elevation change rate at the FIIC is negligible (less than 0.003 m/a [*Wu et al.*, 2010]). Multiplying the volume change rates by the relevant density estimates, we determined the net mass change rate of the FIIC to have been zero (0.0 ± 0.5 Gt/a) during 2002–2009.

[35] We used the RACMO2 output for 1989–2009 to estimate the net SMB of the FIIC during our study period (Figure 4). The annual net SMB values show that the years 2002, 2003 and 2004 are characterized by low net SMB values. Indeed these three years are the three most negative net SMB years between 1989 and 2009. Year 2006, on the other hand, is the second largest net SMB year during this interval. Based on RACMO2, the average annual SMB anomaly (from 1989–2009 mean 73 ± 26 kg/m^2) during the RA-2 study period was −67 ± 25 kg/m^2 a. When interpreting the altimeter data, it has to be remembered that the conditions during the study period were not typical, and in consequence the measured trends do not reflect long term trends.

[36] The temporal resolution of RA-2 allows us to compare the measured elevation changes and modeled net SMB of the FIIC. We compared August-to-August RA-2 elevation changes with RACMO2 modeled net SMB over the flat areas of the FIIC (surface slope <3%). Because RA-2 data begin from September 2002, the 2002–2003 value is from September to August. The comparison is presented in Figure 5. The correlation coefficient between the elevation

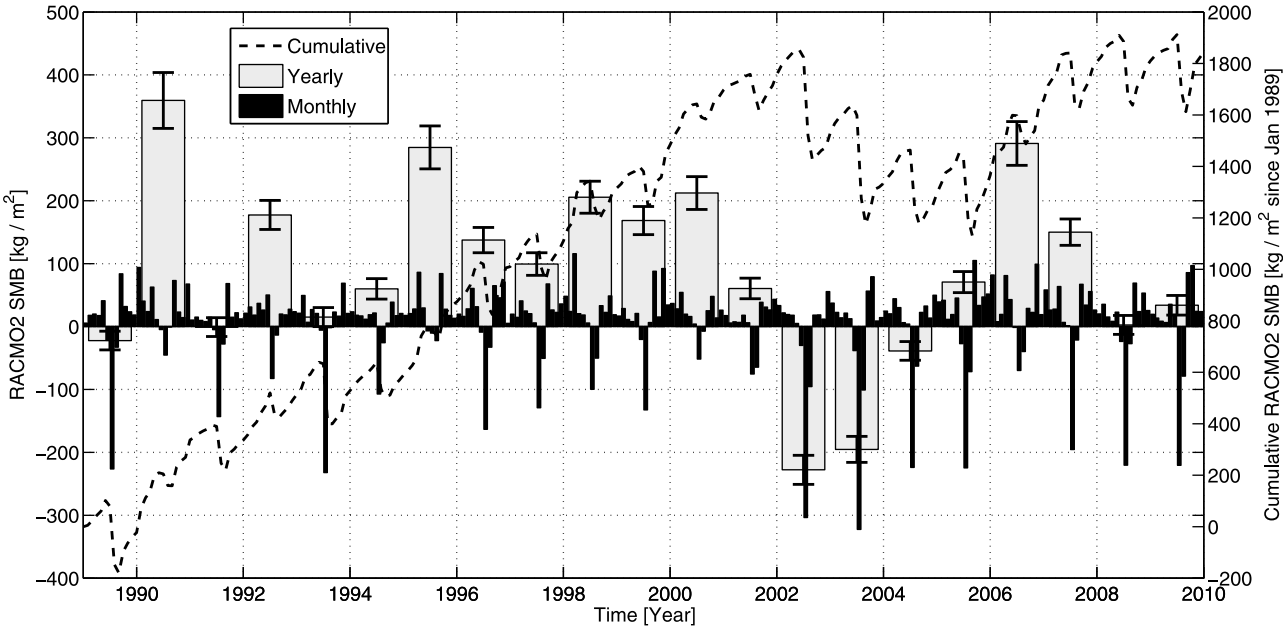

Figure 4. RACMO2 modeled net surface mass balance of the Flade Isblink Ice Cap.

change and the net SMB is $R = 0.94$, and the null hypothesis probability $P = 0.0014$. This suggests that the SMB was the main driver of the elevation change of this area during the RA-2 measurement period.

[37] As discussed before, the surface elevation of the northern dome of the FIIC appears to be driven by ice dynamics (the presence of surge-type glaciers) in addition to changes in the SMB. To test this assumption, we chose two subareas of the flat area – the northern and southern domes (see Figure 1)– for closer study. We compared annual RA-2 elevation changes with the RACMO2 modeled annual net SMB on these subareas (Figure 5). Measured annual elevation change and modeled SMB correlate strongly in the southern dome (Figure 5, middle): $R = 0.97$ and $P = 0.0004$. This suggest that changes in the surface elevation of the southern dome of the FIIC were driven by the net SMB. This is an expected result since *Palmer et al.* [2010] have showed that this area has only few slow flowing outlet glaciers. Strong correlation of SMB and elevation change also implies that the interannual variation of firn compaction rate is small.

[38] In the northern dome area (Figure 5, right) the correlation between SMB and surface elevation change is not present ($R = 0.38$, $P = 0.40$). In fact, at the northern dome we observe a year with negative net SMB and positive elevation change (2002–2003), as well as a year with large positive net SMB and elevation loss (2006–2007). As the surface geometry of the northern dome is similar to the southern dome, there is no reason to suspect that the misfit is due to measurement errors. Similarly, we have no reason to expect that RACMO2 would perform differently in the northern dome than in other flat areas of the FIIC. Instead,

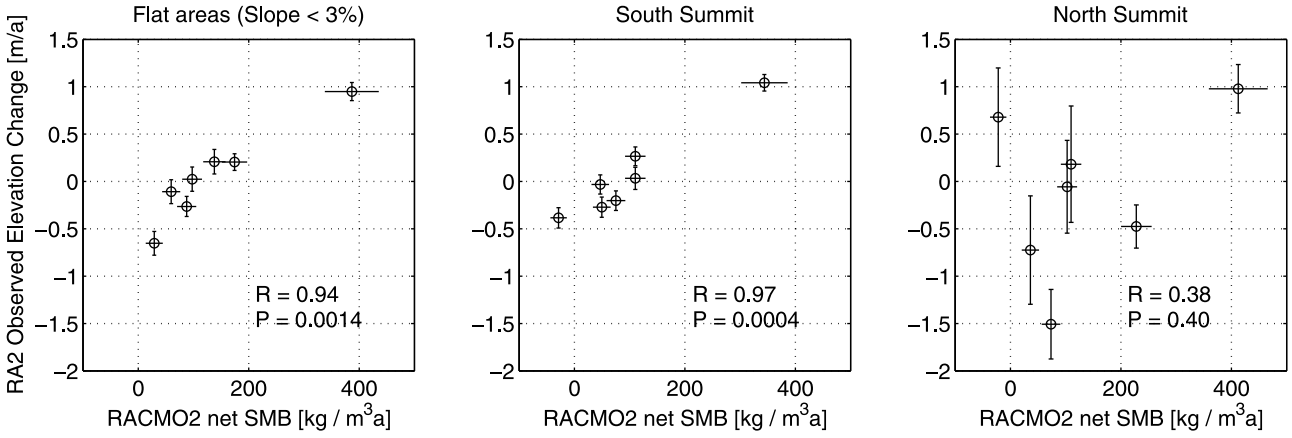

Figure 5. Comparison of RACMO2 modeled net SMB and RA-2 measured elevation change. Points are August to August (except 2002–2003 September–August) (left) Areas of the FIIC with slope <3%. (middle) South Summit. (right) North Summit.

the lack of correlation could be explained by interannual variation of ice flow from this area, or variation in the firn compaction rate. The variable ice flow in this area is supported by observed glacier slowdown [*Joughin et al.*, 2010]. As we have no measurements of firn compaction rates in the area, we cannot rule out a contribution from variable firn compaction to the observed surface elevation changes of the northern dome, although such a contribution is not observed in the southern dome.

[39] Overall zero mass change rate is an unexpected result, since during our study period the GrIS was losing mass at a rate of approximately 200 Gt/a [*Rignot et al.*, 2011]. Most of this mass loss was due to changes around the margins of the GrIS – areas similar to FIIC. However, much of the elevation loss on GrIS is dynamically-driven [*Pritchard et al.*, 2009]. We see no such thinning on the FIIC, where elevation changes seems to be driven mostly by SMB. Based on the RACMO2/SMB comparison above, the surface elevation is dynamically-driven only in the northwest outlet glaciers of the FIIC and their drain area (northern dome). Furthermore, the only significant dynamic event during our observation period is a slowdown of these glaciers, resulting into thickening. Thus the data implies, somewhat surprisingly, that FIIC is responding to the changing climate in a different manner than the GrIS.

4. Conclusions

[40] 1. The average surface elevation change rate of the FIIC has been near zero (0.03 ± 0.03 m/a) between September 2002 and September 2009. In consequence, during this period the mass change rate of the FIIC has been zero (0.0 ± 0.5 Gt/a), assuming changes in volume above and below the LSSL occurred at the density of firn and ice, respectively.

[41] 2. The GLAS-observed local elevation change rates during 2004–2008 range from 3.4 ± 0.7 m/a to -2.5 ± 0.7 m/a. The maximum value is among the fastest thickening reported anywhere in Greenland.

[42] 3. Both RA-2 and GLAS show the same spatial elevation change rate pattern: areas above late summer snow line were gaining elevation (on average 0.09 ± 0.04 m/a between 2002–2009 based on RA-2 measurements) and areas below late summer snow line were losing elevation (on average -0.16 ± 0.05 m/a between 2002 and 2009 based on RA-2 measurements).

[43] 4. In the flat regions of the FIIC, the overall surface elevation changes can be explained by annual variations in the net SMB. At the northern dome of the FIIC, net SMB does not explain the observed elevation changes. This is likely the result of a continuation of the surge phase of the outlet glaciers in this region.

[44] **Acknowledgments.** This work has been undertaken as part of the ESA GlobGlacier project (21088/07/I-EC) (http://globglacier.ch/). The authors wish to thank Gabriele Bippus from ENVEO IT for the LSSL of the FIIC.

References

Arthern, R., D. Wingham, and A. Ridout (2001), Controls on ERS altimeter measurements over ice sheets: Footprint-scale topography, backscatter fluctuations, and the dependence of microwave penetration depth on satellite orientation, *J. Geophys. Res.*, *106*(D24), 33,471–33,484.

Bougamont, M., J. L. Bamber, and W. Greuell (2005), A surface mass balance model for the Greenland Ice Sheet, *J. Geophys. Res.*, *110*, F04018, doi:10.1029/2005JF000348.

Copland, L., M. Sharp, and J. Dowdeswell (2003), The distribution and flow characteristics of surge-type glaciers in the Canadian High Arctic, *Ann. Glaciol.*, *36*, 73–81.

Ettema, J., M. R. van den Broeke, E. van Meijgaard, W. J. van de Berg, J. L. Bamber, J. E. Box, and R. C. Bales (2009), Higher surface mass balance of the Greenland ice sheet revealed by high-resolution climate modeling, *Geophys. Res. Lett.*, *36*, L12501, doi:10.1029/2009GL038110.

Ettema, J., M. R. van den Broeke, E. van Meijgaard, W. J. van de Berg, J. E. Box, and K. Steffen (2010), Climate of the Greenland ice sheet using a high-resolution climate model–Part 1: Evaluation, *Cryosphere Discuss.*, *4*, 561–602.

Gardner, A. S., G. Moholdt, B. Wouters, G. J. Wolken, D. O. Burgess, M. J. Sharp, J. G. Cogley, C. Braun, and C. Labine (2011), Sharply increased mass loss from glaciers and ice caps in the Canadian Arctic Archipelago, *Nature*, *473*, 357–360, doi:10.1038/nature10089.

Hall, D. K., J. E. Box, K. A. Casey, S. J. Hook, C. A. Shuman, and K. Steffen (2008), Comparison of satellite-derived and in-situ observations of ice and snow surface temperatures over Greenland, *Remote Sens. Environ.*, *112*(10), 3739–3749, doi:10.1016/j.rse.2008.05.007.

Hjort, C. (1997), Glaciation, climate history, changing marine levels and the evolution of the Northeast Water Polynya, *J. Mar. Syst.*, *10*(1–4), 23–33.

Joughin, I., B. E. Smith, I. M. Howat, T. Scambos, and T. Moon (2010), Greenland flow variability from ice-sheet-wide velocity mapping, *J. Glaciol.*, *56*(197), 415–430.

Kelly, M. A., and T. V. Lowell (2009), Fluctuations of local glaciers in Greenland during latest Pleistocene and Holocene time, *Quat. Sci. Rev.*, *28*(21–22), 2088–2106, doi:10.1016/j.quascirev.2008.12.008.

Krabill, W., et al. (2000), Greenland ice sheet: High-elevation balance and peripheral thinning, *Science*, *289*(5478), 428–430.

Meier, M. F., M. B. Dyurgerov, U. K. Rick, S. O'Neel, W. T. Pfeffer, R. S. Anderson, S. P. Anderson, and A. F. Glazovsky (2007), Glaciers dominate Eustatic sea-level rise in the 21st century, *Science*, *317*(5841), 1064–1067, doi:10.1126/science.1143906.

Nielsen, C., R. Forsberg, S. Ekholm, and J. Mohr (1997), Merging of elevations from SAR interferometry, satellite altimetry, GPS and laser altimetry in Greenland, in *Third ERS Symposium on Space at the Service of our Environment*, vol. 1, *Eur. Space Agency Spec. Publ.*, vol. 414, pp. 415–420, Eur. Space Agency, Noordwijk, Netherlands.

Palmer, S., A. Shepherd, A. Sundal, E. Rinne, and P. Nienow (2010), InSAR observations of ice elevation and velocity fluctuations of the Flade Isblink ice cap, Eastern North Greenland, *J. Geophys. Res.*, *115*, F04037, doi:10.1029/2010JF001686.

Pritchard, H. D., R. J. Arthern, D. G. Vaughan, and L. A. Edwards (2009), Extensive dynamic thinning on the margins of the Greenland and Antarctic ice sheets, *Nature*, *461*(7266), 971–975, doi:10.1038/nature08471.

Radić, V., and R. Hock (2010), Regional and global volumes of glaciers derived from statistical upscaling of glacier inventory data, *J. Geophys. Res.*, *115*, F01010, doi:10.1029/2009JF001373.

Rasmussen, L. (2004), Set fra oven: Et hjorne af gronland, *Verjet*, *100*, 17–20.

Resti, A., J. Benveniste, M. Roca, and G. Levrini (1999), The Envisat Radar Altimeter System (RA-2), *ESA Bull.*, *98*, 94–101.

Rignot, E., I. Velicogna, M. R. van den Broeke, A. Monaghan, and J. Lenaerts (2011), Acceleration of the contribution of the Greenland and Antarctic ice sheets to sea level rise, *Geophys. Res. Lett.*, *38*, L05503, doi:10.1029/2011GL046583.

Rinne, E., A. Shepherd, A. Muir, and D. Wingham (2011), A comparison of recent elevation change estimates of the Devon Ice Cap as measured by the ICESat and EnviSAT satellite altimeters, *IEEE Trans. Geosci. Remote Sens.*, *49*(6), 1902–1910.

Sandwell, D. (1987), Biharmonic spline interpolation of GEOS-3 and SEASAT altimeter data, *Geophys. Res. Lett.*, *14*(2), 139–142, doi:10.1029/GL014i002p00139.

Soussi, B., and P. Femenias (2006), ENVISAT RA-2/MWR Level 2 User Manual, user manual, Eur. Space Agency, Noordwijk, Netherlands.

Thomas, R., C. Davis, E. Frederick, W. Krabill, Y. Li, S. Manizade, and C. Martin (2008), A comparison of Greenland ice-sheet volume changes derived from altimetry measurements, *J. Glaciol.*, *54*(185), 203–212.

van den Broeke, M., J. Bamber, J. Ettema, E. Rignot, E. Schrama, W. J. van de Berg, E. van Meijgaard, I. Velicogna, and B. Wouters (2009), Partitioning recent Greenland mass loss, *Science*, *326*(5955), 984–986, doi:10.1126/science.1178176.

Wingham, D., A. Ridout, R. Scharroo, R. Arthern, and C. Shum (1998), Antarctic elevation change from 1992 to 1996, *Science*, *282*(5388), 456–458.

Wu, X., M. B. Heflin, H. Schotman, B. L. A. Vermeersen, D. Dong, R. S. Gross, E. R. Ivins, A. Moore, and S. E. Owen (2010), Simultaneous estimation of global present-day water transport and glacial isostatic adjustment, *Nat. Geosci.*, *3*(9), 642–646, doi:10.1038/ngeo938.

Zwally, H., A. Brenner, J. Major, R. Bindchlader, and J. Marsh (1989), Growth of Greenland Ice Sheet: Measurement, *Science*, *246*(4937), 1587–1589.

Zwally, H., et al. (2002), ICESat's laser measurements of polar ice, atmosphere, ocean, and land, *J. Geodyn.*, *34*(3–4), 405–445.

Zwally, H., R. Schutz, C. Bentley, J. Bufton, T. Herring, J. Minster, J. Spinhirne, and R. Thomas (2003), *GLAS/ICESat L1B Global Elevation Data V018*, 15 Oct. to 18 Nov. 2003, http://nsidc.org/data/gla06.html, Natl. Snow and Ice Data Cent., Boulder, Colo. [Updated 2009.]

Zwally, H. J., M. B. Giovinetto, J. Li, H. G. Cornejo, M. A. Beckley, A. C. Brenner, J. L. Saba, and D. Yi (2005), Mass changes of the Greenland and Antarctic ice sheets and shelves and contributions to sea-level rise: 1992–2002, *J. Glaciol.*, *51*(175), 509–527.

Zwally, H. J., et al. (2011), Greenland ice sheet mass balance: distribution of increased mass loss with climate warming; 2003–07 versus 1992–2002, *J. Glaciol.*, *57*(201), 88–102.

J. Ettema, Faculty of Geo-Information Science and Earth Observation, University of Twente, PO Box 219, NL-7500 AE Enschede, Netherlands.

A. Muir and D. Wingham, Centre for Polar Observation and Modeling, University College of London, Gower Street, London WC1E 6BT, UK.

S. Palmer and A. Shepherd, School of Earth and Environment, University of Leeds, Leeds LS2 9JT, UK.

E. Rinne, School of GeoSciences, University of Edinburgh, Drummond Street, Edinburgh EH8 9XP, UK. (eero.rinne@ed.ac.uk)

M. R. van den Broeke, Institute for Marine and Atmospheric Research, Utrecht University, Princetonplein 5, NL-3584 CC Utrecht, Netherlands.